Jahn-Teller effect in the fluorescent level of Mn^{++} in ZnSe and ZnS

R. Parrot, C. Naud, and C. Porte

Universite P. et M. Curie, Laboratoire de Luminescence, 4 Place Jussieu, 75230 Paris Cedex 05, France*

D. Fournier, A. C. Boccara, and J. C. Rivoal

Laboratoire d'Optique Physique, Ecole de Physique et Chimie Industriells,† 10 rue Vauquelin, 75231 Paris Cedex 05, France

(Received 22 September 1976)

Uniaxial-stress experiments have been used to analyze the fine-structure lines of the lowest $^4T_1$ level of Mn^{++} in cubic ZnSe and in cubic ZnS containing stacking faults. We show that the two fine-structure lines due to the cubic centers in ZnSe and ZnS can be interpreted by Ham's model corresponding to a strong Jahn-Teller coupling with E symmetry modes. In both cases, the observed lines correspond to transitions from the $|^6A_1\rangle$ fundamental state to the almost degenerate states $|\Gamma_7\rangle,(3/\sqrt{10})|\Gamma_8(3/2)\rangle - (1/\sqrt{10})|\Gamma_8(5/2)\rangle$ for the line at lower energy and $|\Gamma_6\rangle,(1/\sqrt{10})|\Gamma_8(3/2)\rangle + (3/\sqrt{10})|\Gamma_8(5/2)\rangle$ for the line at higher energy. The influence of the Jahn-Teller effect on the axial Mn^{++} centers in stacking faults of ZnS is also briefly considered. Finally a comparison is made of the Jahn-Teller effect in the lowest $^4T_1$ and $^4T_2$ states of Mn^{++} in ZnS and ZnSe.

I. INTRODUCTION

Although the Jahn-Teller effect has been extensively studied for a number of d ions either by electron paramagnetic resonance or by optical spectroscopy,[1] very few detailed studies of this effect for d^5 ions have been reported. Furthermore, to our knowledge, only Mn^{++} has been studied among the d^5 ions.

Amongst the early studies on the Jahn-Teller effect on Mn^{++} ions, we can cite a theoretical study of this effect on the fluorescent level of Mn^{++} in[2] $MgOAl_2O_3$ and also a theoretical determination of the g factors of the fine-structure lines of the fluorescent $^4T_1$ level of Mn^{++} in ZnS in the case of a strong coupling to an E vibrational mode.[3] However, no direct demonstration of the nature of the coupling, either to E symmetry modes or T_2 symmetry modes of both was undertaken at that time.

The first systematic study of the Jahn-Teller effect on Mn^{++} was made by Chen, McClure, and Solomon[4] and Solomon and McClure[5] who studied the orbital triplet levels $^4T_1$ and $^4T_2$ at lower energy of Mn^{++} in antiferromagnetic $RbMnF_3$. These authors interpreted all their experimental results on the Zeeman levels using Ham's formalism corresponding to a strong Jahn-Teller coupling to E symmetry modes and to a small coupling to a T_2 vibrational mode for certain levels.

More recently, a study of the Jahn-Teller effect in the lowest $^4T_2$ level of Mn^{++} in ZnSe and ZnS has been published.[6] It was clearly shown that the zero-pressure spectrum could lead to the erroneous conclusion that a strong coupling to E modes is present. By means of uniaxial stress experiments, it was demonstrated that the $^4T_2$ level is subjected to a medium Jahn-Teller coupling to an E symmetry mode and that the intensity of one

TABLE I. Dimensions and orientations of the crystals used in our experiments. S is the cross-sectional area perpendicular to the applied pressure $\vec{P}$. 8% of Mn^{++} ions in ZnS are in stacking faults, the other ions are in cubic sites.

Sample	Dimensions (mm) (error ± 0.01 mm)	S (mm^2)	Applied pressure
ZnSe: Mn			
(Semielements)	1.50×2.75×3.55	4.12	$\vec{P}\parallel[001]$
0.1-mol% Mn	1.85×1.92×4.87	3.55	$\vec{P}\parallel[110]$
cubic	2.70×3.45×3.55	9.31	$\vec{P}\parallel[111]$
ZnS: Mn			
(Eagle Picher)	1.61×1.95×4.50	3.14	$\vec{P}\parallel[1\bar{1}0]_W$
0.01-mol% Mn cubic plus stacking faults	0.82×1.23×3.16	1.01	$\vec{P}\parallel[111]_W$

fine-structure line is transferred selectively to excited vibronic levels. In fact, the selective intensity transfer has been rarely studied. Among the very few studies of this effect, we can cite, for example, the work of Ham and Slack[7] who demonstrated the presence of an intensity transfer to one-phonon sidebands in the $^5T_2$ state of Fe^{2+} in ZnS.

Very recently a theoretical investigation based on the hypothesis of a strong Jahn-Teller coupling of several triplet levels of Mn^{++} in various compounds has been made by Koidl.[8] A study of the Zeeman effect and of the magnetic polarization in the fluorescent $^4T_1$ level of Mn^{++} in ZnS has been performed by Fournier *et al.*[9]; their calculations of the splitting and of the intensities of the zero-phonon lines computed in the hypothesis of a strong coupling were in good accordance with the experimental data. The main purpose of this paper is to confirm directly the hypothesis of a strong Jahn-Teller coupling to an E mode of the fluorescent level of Mn^{++} in ZnS and to determine the nature of the coupling in the case of Mn^{++} in ZnSe.

The excitation spectra under zero-pressure and the uniaxial stress experiments are reported in Sec. II. The splittings under stresses of the two fine-structure lines of the fluorescent $^4T_1$ level of Mn^{++} in ZnSe and in the cubic sites of ZnS will show that this level is strongly coupled to an E vibrational mode, the coupling to the T_2 modes being negligible. In Sec. III, we briefly recall Ham's model for an orbital triplet state coupled to an E vibrational mode, and we give several formulas permitting convenient calculation for the second-order spin-orbit interaction (extended to the entire d^5 configuration) for the relative dipole strengths and for the polarization effects under stresses. It is shown in Sec. IV that all experimental results (stress and Zeeman experiment) for Mn^{++} in ZnSe and in cubic ZnS are correctly described by assuming an almost complete quenching of the first-order spin-orbit interaction. Finally, the couplings of the lowest $^4T_1$ and $^4T_2$ states of Mn^{++} in ZnSe and ZnS are compared in Sec. V.

II. EXPERIMENTS

A. Samples and apparatus

The origin, the concentration, and the crystallographic structure of the ZnSe: Mn and ZnS: Mn samples used in our experiments are identical to those described in preceding papers.[6,10] These characteristics together with the dimensions and orientations of the crystals are given in Table I.

Owing to the small absorption coefficient of the $^6A_1 \rightarrow {}^4T_1$ band of Mn^{++} in ZnSe and ZnS, we per-

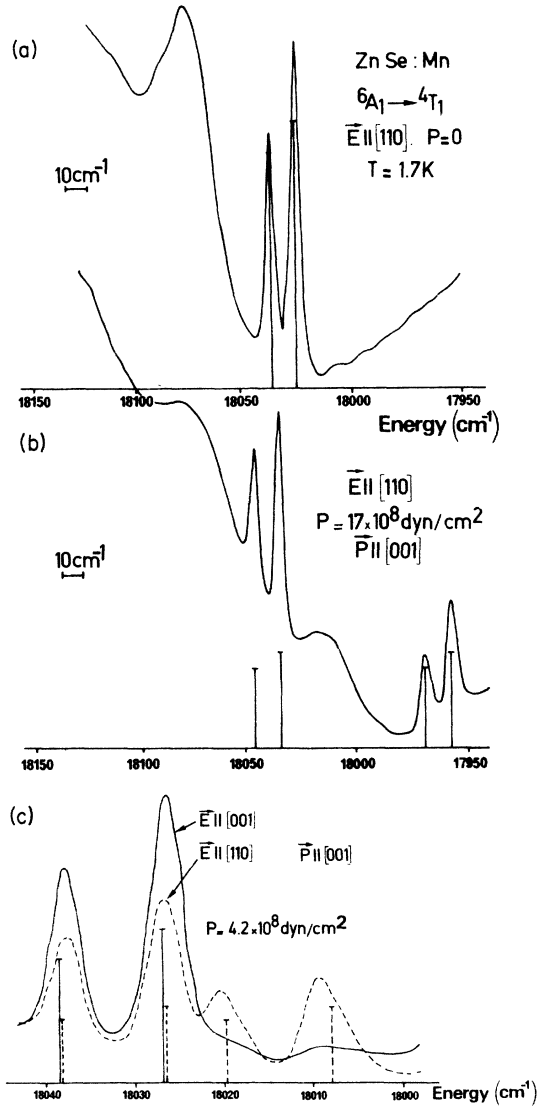

FIG. 1. (a) Excitation spectrum of the fluorescent $^4T_1$ level of Mn^{++} in ZnSe; (b) uniaxial stress effect for the maximum applied pressure ($\vec{P} \parallel [001]$) and (c) polarization effects. In (a) the linewidths of the two zero-phonon lines are 4.5 cm^{-1}. The phonon assisted line appears at 18 075 cm^{-1}. In (b) the linewidths of the zero-phonon lines are, respectively, 6 cm^{-1} for the two lines at lower energy, and 4.5 cm^{-1} for the two lines at higher energy. The splittings of the zero-phonon lines and of the phonon-assisted line are equal to 70 cm^{-1}. These spectra were obtained for the electric field $\vec{E}$ of the excitation light parallel to a [110] axis. The vertical lines represent the calculated relative dipole strengths as given by the model of Secs. III and IV. The broken-line spectra (c) were obtained for the electric field of the excitation light parallel to a [110] axis. The continuous line spectra correspond to $\vec{E} \parallel [001]$. The vertical lines give the positions and the calculated relative dipole strengths of the zero-phonon lines. Only two lines are observed when $\vec{E} \parallel [001]$ while four lines appear when $\vec{E} \parallel [110]$.

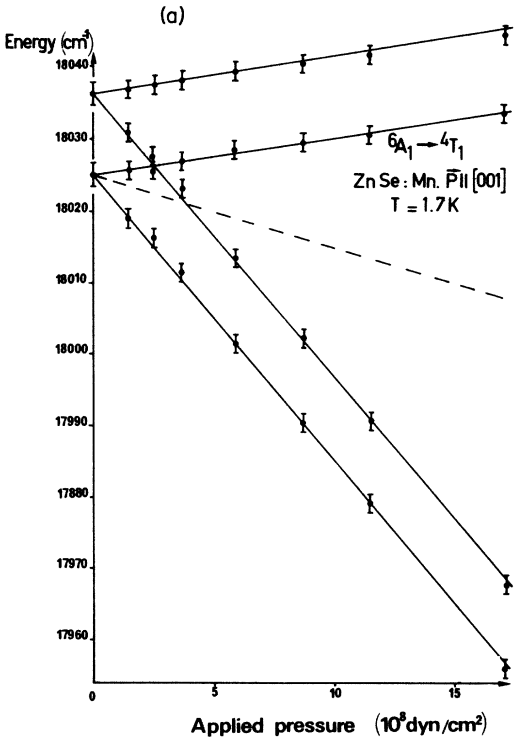

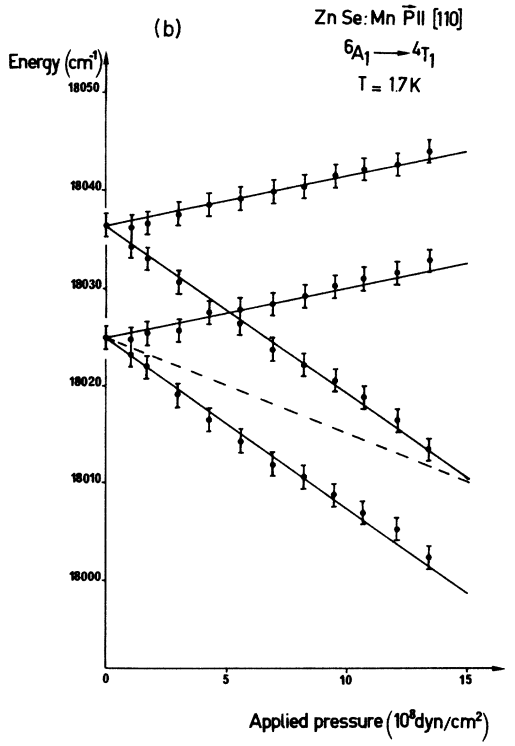

formed excitation experiments. The excitation spectra were obtained by scanning the absorption spectra at variable wavelengths with a dye laser and detecting the light emitted by the tail of the emission band. The excitation light is given by a CR5 laser associated with a dye laser (model 490 manufactured by Coherent Radiation, the dye being rhodamine 110). The light emitted by the crystals is filtered by an interference filter (Matra HDL-TDO Vis., bandwidth: 260 Å, maximum transparency at 5990 Å) and sent on a photomultiplier. A Fabry-Perot spectrometer permitted measuring the splittings and shifts of the absorption lines.

The experiments were performed at 1.7 K, the crystals being immersed in liquid helium. The pressure was applied as previously described.[6]

B. Experimental results

The absorption spectra of Mn^{++} in ZnSe for a zero applied pressure and for the maximum applied pressure ($\vec{P} \| [001]$, $P = 17 \times 10^8$ dyn/cm^2) are given in Figs. 1(a) and 1(b).

For $\vec{P} = 0$, two zero-phonon lines separated by 11.5 ± 0.5 cm^{-1} appear clearly in the spectrum. The line at lower energy appears at $18\,025 \pm 2$ cm^{-1}. This last result is in agreement with Langer and Richter[11] who observed an emission line at 18 025 cm^{-1}; however, the energy separations between the zero-phonon lines are in disagreement (11.5 cm^{-1} in our experiment and 20 cm^{-1} in the experiment of Langer and Richter). A well-defined phonon-assisted line is observed at 18 075 cm^{-1} and a broad band appears at higher energy.

When a pressure is applied along a [001] axis, each zero-phonon line is split into two components.

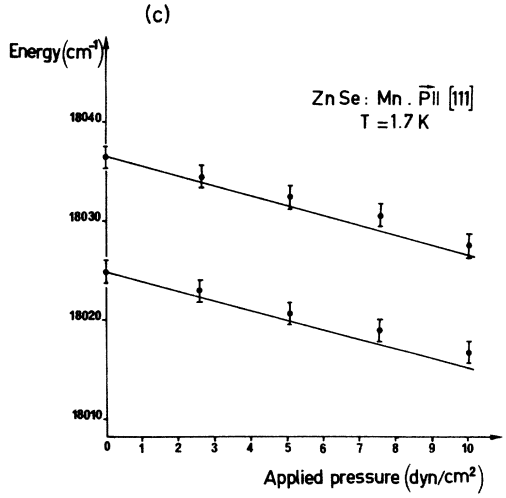

FIG. 2. ZnSe : Mn. Splittings and shifts in terms of the applied pressure: (a) $\vec{P} \| [001]$; (b) $\vec{P} \| [110]$; (c) $\vec{P} \| [111]$. The dotted lines represent the shifts due to the $\epsilon(A_1)$ strains. $\vec{E} \| [110]$. The curves are drawn from the values of the parameters given in Sec. IV.

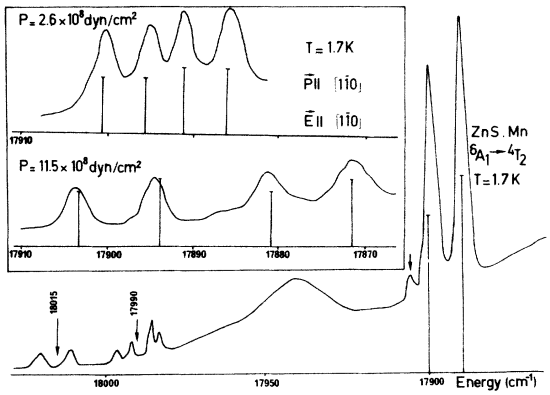

FIG. 3. Excitation spectrum of the $^4T_1$ level of Mn^{++} in ZnS. $P=0$. The two zero-phonon lines at 17 900 cm^{-1} and 17 890 cm^{-1} correspond to Mn^{++} in cubic sites. The line at 17 905 cm^{-1}, the four lines centered at 17 990 cm^{-1}, and the two lines centered at 18 015 cm^{-1} are zero-phonon lines of Mn^{++} in stacking faults. The insert represents the uniaxial stress effect on the zero-phonon lines of Mn^{++} in cubic sites: $\vec{P} \parallel [1\bar{1}0]$, $\vec{E} \parallel [1\bar{1}0]$.

An overall view of the absorption spectrum for the maximum applied pressure ($P = 17 \times 10^8$ dyn/cm^2) is given in Fig. 1(b). Two sets of two lines separated by 75 cm^{-1} are observed in this figure. Clear polarization effects are observed, even for the smallest applied pressure ($P = 1.4 \times 10^8$ dyn/cm^2). Figure 1(c) shows spectra obtained for $\vec{P} \parallel [100]$ and for the electric field of the excitation light parallel to a [100] axis and to a [110] axis.

The shifts and splittings of the zero-phonon lines are represented in terms of the applied pressure in Fig. 2. No splitting and no broadening of the zero-phonon lines are observed when $\vec{P} \parallel [111]$ even for the maximum applied pressure $P = 10.5 \times 10^8$ dyn/cm^2 [see Fig. 2(c)].

In the case of ZnS : Mn, the absorption spectra for $P = 0$ are identical to those reported by Fournier *et al.*[9] (Fig. 3). Two zero-phonon lines are observed at 17 900 and 17 890 cm^{-1} (these values are in agreement with those reported by Zigone *et al.*[12] at 17 900.5 cm^{-1} and 17 891 cm^{-1}). Two groups of lines centered at 17 990 and 18 015 cm^{-1} have been associated with the zero-phonon lines of axial Mn^{++} centers in stacking faults.

The insert in Fig. 3 shows the influence of an applied pressure $\vec{P} \parallel [1\bar{1}0]$ on the zero-phonon lines of Mn^{++} ions in cubic sites. Figure 4 represents the shifts and splittings of the zero-phonon lines in terms of the applied pressure. The behavior of these lines is analogous to that of Mn^{++} in ZnSe in the sense that each line is split into two components. For $\vec{P} \parallel [111]$, we observed a slight broadening of the cubic lines, however, due to the smallness of the sample used for this experiment (see

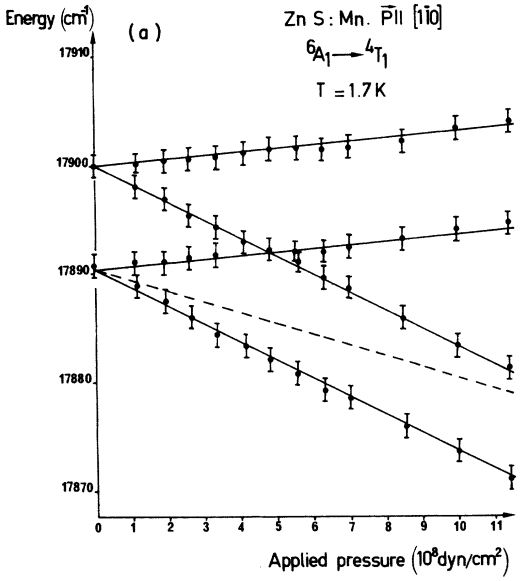

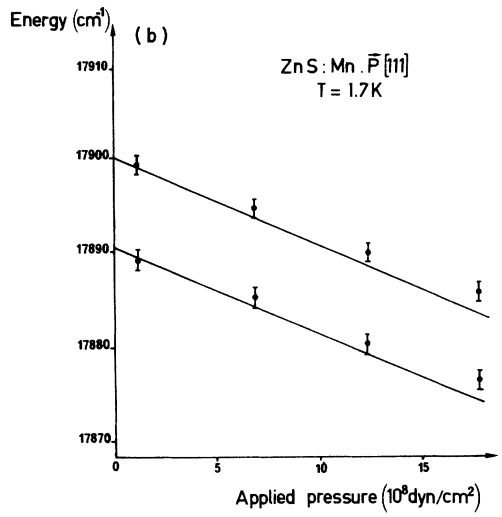

FIG. 4. ZnS : Mn. Splittings and shifts of the zero-phonon lines of Mn^{++} in cubic sites in terms of the applied pressure. $\vec{P} \parallel [1\bar{1}0]$ and $\vec{P} \parallel [111]$. The dotted lines represent the shifts due to the $\epsilon(A_1)$ strains. The curves are drawn from the values of the parameters given in Sec. IV.

Table I), this broadening could be due to a misorientation of the crystal.

All these effects clearly indicate that there is a strong coupling of the $^4T_1$ relaxed levels to a E Jahn-Teller active mode.

Uniaxial stress experiments performed on the zero-phonon lines of Mn^{++} in stacking faults (Fig. 5) showed that the two lines at 18 012 and 18 022 cm^{-1} are split into two components for $\vec{P} \parallel [1\bar{1}0]$, the shifts and splittings being identical to those

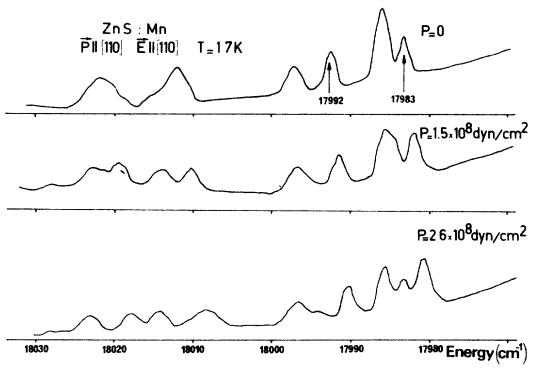

FIG. 5. ZnS:Mn. Uniaxial stress effects on the zero-phonon lines of Mn^{++} in stacking faults. The behavior of the lines centered at 18 015 cm^{-1} is identical to that of the lines of Mn^{++} in cubic sites (for $P=2.6\times10^8$ dyn/cm^2, the splittings and shifts are identical to those reported in Fig. 3 for the same pressure). The behavior of the four lines centered at 17 990 cm^{-1} is more complicated. The two lines at 17 983 and 17 992 cm^{-1} are split and shifted, while no splitting of the two other lines is observed.

observed for the cubic lines. The behavior of the four lines centered at 17 980 cm^{-1} is more complicated; the two lines at 17 983 and 17 992 cm^{-1} are not split but shifted, while the two other lines are split into two components.

III. JAHN-TELLER EFFECT

A. Jahn-Teller coupling to an E vibrational mode. Energy levels in Td symmetry

Since the case of a strong coupling to an E vibrational mode has been extensively studied by Ham,[1,13] we will only recall the main results of the theory and give the relevant formulas for the lowest $^4T_1$ level of d^5 ions in cubic symmetry.

The first-order spin-orbit interaction $\mathcal{H}_{SO}$ acting on the fundamental vibronic state can be replaced by the following equivalent operator $\mathcal{H}_{SO}^{(1)}$ acting on the electronic states:

$$\mathcal{H}_{SO}^{(1)} = e^{-3E_{JT}/2\hbar\omega}\mathcal{H}_{SO}\,,$$

where E_{JT} is related to the strength of the Jahn-Teller coupling V_E and to the angular frequency of the effective mode of E symmetry by

$$E_{JT} = V^2/2\mu\omega^2\,,$$

μ being the mass of the effective phonon.

The matrix elements of the second-order spin-orbit interactions in the fundamental vibronic level are given by

$$\langle {}^4T_{1j},00|\mathcal{H}_{SO}^2|{}^4T_{1j},00\rangle = -\left(\frac{f_b}{\hbar\omega}\right)\sum_{i\neq j}\langle {}^4T_{1j}|\mathcal{H}_{SO}|{}^4T_{1i}\rangle\langle {}^4T_{1i}|\mathcal{H}_{SO}|{}^4T_{1j}\rangle + \sum_{^{2S+1}h}\frac{\langle {}^4T_{1j}|\mathcal{H}_{SO}|{}^{2S+1}h\rangle\langle {}^{2S+1}h|\mathcal{H}_{SO}|{}^4T_{1j}\rangle}{W({}^4T_1)-W({}^{2S+1}h)}$$

for the diagonal matrix elements, and

$$\langle {}^4T_{1j},00|\mathcal{H}_{SO}^2|{}^4T_{1k},00\rangle = -\left(\frac{f_a}{\hbar\omega}\right)\langle {}^4T_{1j}|\mathcal{H}_{SO}|{}^4T_{1i}\rangle\langle {}^4T_{1i}|\mathcal{H}_{SO}|{}^4T_{1k}\rangle + e^{-x/2}\sum_{^{2S+1}h}\frac{\langle {}^4T_{1j}|\mathcal{H}_{SO}|{}^{2S+1}h\rangle\langle {}^{2S+1}h|\mathcal{H}_{SO}|{}^4T_{1k}\rangle}{W({}^4T_1)-W({}^{2S+1}h)}$$

for the off-diagonal matrix elements;

$$f_b = e^{-x}G(x),\quad \text{with}\quad x=3E_{JT}/\hbar\omega,\quad G(x)=\sum_{n=1}^{\infty}\frac{x^n}{n(n!)},\quad \text{and}\quad f_a = e^{-x}G(\tfrac{1}{2}x)\,.$$

Following the method previously described,[6] the diagonal and off-diagonal matrix elements of $\mathcal{H}_{SO}^2$ (in the real tetragonal component system $^{2S+1}hM\theta$ defined by Griffith[14]) were calculated in terms of the classical matrix elements in Td* by the following relations:

$$\langle\Gamma_6|\mathcal{H}_{SO}^2|\Gamma_6\rangle_{diag} = \tfrac{1}{3}\langle\Gamma_6|\mathcal{H}_{SO}^2|\Gamma_6\rangle + \tfrac{1}{15}\langle\Gamma_8(\tfrac{3}{2})|\mathcal{H}_{SO}^2|\Gamma_8(\tfrac{3}{2})\rangle + \tfrac{3}{5}\langle\Gamma_8(\tfrac{5}{2})|\mathcal{H}_{SO}^2|\Gamma_8(\tfrac{5}{2})\rangle + \tfrac{2}{5}\langle\Gamma_8(\tfrac{3}{2})|\mathcal{H}_{SO}^2|\Gamma_8(\tfrac{5}{2})\rangle\,,$$

$$\langle\Gamma_7|\mathcal{H}_{SO}^2|\Gamma_7\rangle_{diag} = \tfrac{1}{3}\langle\Gamma_7|\mathcal{H}_{SO}^2|\Gamma_7\rangle + \tfrac{3}{5}\langle\Gamma_8(\tfrac{3}{2})|\mathcal{H}_{SO}^2|\Gamma_8(\tfrac{3}{2})\rangle + \tfrac{1}{15}\langle\Gamma_8(\tfrac{5}{2})|\mathcal{H}_{SO}^2|\Gamma_8(\tfrac{5}{2})\rangle - \tfrac{2}{5}\langle\Gamma_8(\tfrac{3}{2})|\mathcal{H}_{SO}^2|\Gamma_8(\tfrac{5}{2})\rangle\,,$$

$$\langle\Gamma_8(\tfrac{3}{2})|\mathcal{H}_{SO}^2|\Gamma_8(\tfrac{3}{2})\rangle_{diag} = \tfrac{3}{10}\langle\Gamma_7|\mathcal{H}_{SO}^2|\Gamma_7\rangle + \tfrac{1}{30}\langle\Gamma_6|\mathcal{H}_{SO}^2|\Gamma_6\rangle + \tfrac{41}{75}\langle\Gamma_8(\tfrac{3}{2})|\mathcal{H}_{SO}^2|\Gamma_8(\tfrac{3}{2})\rangle + \tfrac{3}{25}\langle\Gamma_8(\tfrac{5}{2})|\mathcal{H}_{SO}^2|\Gamma_8(\tfrac{5}{2})\rangle - \tfrac{8}{25}\langle\Gamma_8(\tfrac{3}{2})|\mathcal{H}_{SO}^2|\Gamma_8(\tfrac{5}{2})\rangle\,,$$

$$\langle\Gamma_8(\tfrac{5}{2})|\mathcal{H}_{SO}^2|\Gamma_8(\tfrac{5}{2})\rangle_{diag} = \tfrac{1}{30}\langle\Gamma_7|\mathcal{H}_{SO}^2|\Gamma_7\rangle + \tfrac{3}{10}\langle\Gamma_6|\mathcal{H}_{SO}^2|\Gamma_6\rangle + \tfrac{3}{25}\langle\Gamma_8(\tfrac{3}{2})|\mathcal{H}_{SO}^2|\Gamma_8(\tfrac{3}{2})\rangle + \tfrac{41}{75}\langle\Gamma_8(\tfrac{5}{2})|\mathcal{H}_{SO}^2|\Gamma_8(\tfrac{5}{2})\rangle + \tfrac{8}{25}\langle\Gamma_8(\tfrac{3}{2})|\mathcal{H}_{SO}^2|\Gamma_8(\tfrac{5}{2})\rangle\,,$$

$$\langle\Gamma_8(\tfrac{3}{2})|\mathcal{H}_{SO}^2|\Gamma_8(\tfrac{5}{2})\rangle_{diag} = -\tfrac{1}{10}\langle\Gamma_7|\mathcal{H}_{SO}^2|\Gamma_7\rangle + \tfrac{1}{10}\langle\Gamma_6|\mathcal{H}_{SO}^2|\Gamma_6\rangle$$
$$-\tfrac{4}{25}\langle\Gamma_8(\tfrac{3}{2})|\mathcal{H}_{SO}^2|\Gamma_8(\tfrac{3}{2})\rangle + \tfrac{4}{25}\langle\Gamma_8(\tfrac{5}{2})|\mathcal{H}_{SO}^2|\Gamma_8(\tfrac{5}{2})\rangle + \tfrac{6}{25}\langle\Gamma_8(\tfrac{3}{2})|\mathcal{H}_{SO}^2|\Gamma_8(\tfrac{5}{2})\rangle ,$$

and

$$\langle t\tau J|\mathcal{H}_{SO}^2|t\tau J'\rangle_{off\text{-}diag} = \langle t\tau J|\mathcal{H}_{SO}^2|t\tau J'\rangle - \langle t\tau J|\mathcal{H}_{SO}^2|t\tau J'\rangle_{diag} .$$

In the case of the lowest orbital triplet level $^4T_1$ of a d^5 ion, 39 multiplets are involved in the calculation of the second-order spin-orbit interaction; they are[15] $^6A_1$, $^4T_1(3)$, $^4T_2(3)$, $^4E(2)$, $^4A_1(1)$, $^2T_1(8)$, $^2T_2(10)$, $^2E(7)$, $^2A_1(4)$ (the numbers in parentheses are the numbers of multiplets of given spin and symmetry). Of course, the contribution of the second-order spin-orbit coupling between different electronic states is identical to that obtained by the method of equivalent operators used, for example, by Koidl.[8]

B. Uniaxial stress effects

For $\vec{P}\|[110]$, $\vec{P}\|[100]$, and $\vec{P}\|[111]$, the nonzero linear combinations of the strain tensor are, respectively,[16]

$$\epsilon(A_1) = (s_{11}+2s_{12})P ,$$
$$\epsilon(E_u) = -(s_{11}-s_{12})P, \quad \epsilon(T_{2\zeta}) = \tfrac{1}{2}s_{44}P ;$$
$$\epsilon(A_1) = (s_{11}+s_{12})P, \quad \epsilon(E_u) = 2(s_{11}-s_{12})P ;$$
$$\epsilon(A_1) = (s_{11}+2s_{12})P, \quad \epsilon(T_{2\xi}) = \epsilon(T_{2\eta}) = \epsilon(T_{2\zeta}) = \tfrac{1}{3}s_{44}P ,$$

where the s_{ij}'s are elastic compliance constants.

In the case of a strong Jahn-Teller coupling to an E vibrational mode, the matrix elements of the vibrations $\Delta V(T_{2i})$ $(i=\xi,\eta,\zeta)$ of the crystal field are reduced by a factor $e^{-3E_{JT}/2\hbar\omega}$ and will be neglected. However, the matrix elements of $\Delta V(E_u)$ are not affected by the coupling to an E mode. The effect of E_u strains will be described in the following in terms of the parameter:

$$\mathcal{C} = -\langle{}^4T_1\|\Delta V(E_u)\|{}^4T_1\rangle/\epsilon(E_u) .$$

C. Polarization effects under pressure

As in the case of the lowest $^4T_2$ level,[6,17] numerous schemes contribute to the dipole strengths of the fine-structure lines of the lowest $^4T_1$ level. However, being primarily interested by the relative dipole strengths (RDS) we will use an equivalent operator to calculate these dipole strengths. For electric dipolar transitions, the simplest equivalent operator relating the $^6A_1$ and $^4T_1$ levels is

$$\mathcal{H}_{d\text{-}e} = W_2^{(11)2} - W_{-2}^{(11)2} ,$$

where the W's are mixed tensor operators of rank 1 for spin and for the orbital momentum. By using these operators, the polarization effects can be simply calculated in terms of the components $(t\tau J)$ of the eigenvectors of the matrix describing the stress effects, for example. The RDS's $\mathcal{G}(\vec{E}\|[001])$, $\mathcal{G}(\vec{E}\|[110])$, and $\mathcal{G}(\vec{E}\|[1\bar{1}0])$ corresponding, respectively, to light polarized along a [100], [110], and [1$\bar{1}$0] axis are given by

$$\mathcal{G}(\vec{E}\|[001]) = (1/N^2)[|(1/\sqrt{3})(\Gamma_6\tfrac{1}{2}) - (1/\sqrt{15})(\Gamma_8\tfrac{3}{2},\tfrac{1}{2}) + (2/\sqrt{15})(\Gamma_8\tfrac{5}{2},\tfrac{1}{2})|^2$$
$$+|-(2/\sqrt{15})(\Gamma_7\tfrac{1}{2}) + \tfrac{1}{5}\sqrt{3}\,(\Gamma_8\tfrac{3}{2},-\tfrac{3}{2}) - (1/5\sqrt{3})(\Gamma_8\tfrac{5}{2},-\tfrac{3}{2})|^2$$
$$+|(2/\sqrt{15})(\Gamma_6\tfrac{1}{2}) + (7/5\sqrt{3})(\Gamma_8\tfrac{3}{2},\tfrac{1}{2}) + (1/5\sqrt{3})(\Gamma_8\tfrac{5}{2},\tfrac{1}{2})|^2] ,$$

$$\mathcal{G}(\vec{E}\|[110]) = \mathcal{G}(\vec{E}\|[1\bar{1}0]) = (1/2N^2)[|(\sqrt{2}/\sqrt{3})(\Gamma_6\tfrac{1}{2}) + (1/\sqrt{30})(\Gamma_8\tfrac{3}{2},\tfrac{1}{2}) - (\sqrt{2}/\sqrt{15})(\Gamma_8\tfrac{5}{2},\tfrac{1}{2})|^2$$
$$+|(1/\sqrt{10})(\Gamma_8\tfrac{3}{2},-\tfrac{3}{2}) - (\sqrt{2}/\sqrt{5})(\Gamma_8\tfrac{5}{2},-\tfrac{3}{2})|^2$$
$$+|-(\sqrt{2}/\sqrt{15})(\Gamma_7\tfrac{1}{2}) + \tfrac{3}{5}(\sqrt{3}/\sqrt{2})(\Gamma_8\tfrac{3}{2},-\tfrac{3}{2}) + (\sqrt{2}/5\sqrt{3})(\Gamma_8\tfrac{5}{2},-\tfrac{3}{2})|^2$$
$$+|-(\sqrt{2}/\sqrt{5})(\Gamma_6\tfrac{1}{2}) + (1/\sqrt{2})(\Gamma_8\tfrac{3}{2},\tfrac{1}{2})|^2$$
$$+|(\sqrt{2}/\sqrt{15})(\Gamma_6\tfrac{1}{2}) + (1/5\sqrt{6})(\Gamma_8\tfrac{3}{2},\tfrac{1}{2}) - (\sqrt{2}/5\sqrt{3})(\Gamma_8\tfrac{5}{2},\tfrac{1}{2})|^2$$
$$+|-(\sqrt{2}/\sqrt{5})(\Gamma_7\tfrac{1}{2}) - (1/\sqrt{2})(\Gamma_8\tfrac{3}{2},-\tfrac{3}{2})|^2] .$$

The above formulas have been obtained by neglecting the small splitting $\Gamma_8(^6A_1) - \Gamma_7(^6A_1) = 3a$ of the fundamental level. ($3a = 23.6\times10^{-4}$ cm^{-1} for Mn^{++} in[18] ZnS and 59.1×10^{-4} cm^{-1} for Mn^{++} in[18] ZnSe.) They are valid in the case of a negligible, a medium, or a strong Jahn-Teller effect. [The important problem is to determine the relevant $(t\tau J)$'s.]

In the case of a negligible or strong Jahn-Teller

TABLE II. Nonreduced first-order (superscript a) and second-order (superscript b) contributions of the spin-orbit interaction to the splittings and shifts of the $^4T_1$ level of Mn^{++} in ZnSe and ZnS. Spin-orbit parameter: $\zeta_{3d} = 300\ cm^{-1}$. The $^4T_1$ level is taken as reference.

ZnSe	Γ_6	Γ_7	$\Gamma_8(\frac{3}{2})$	$\Gamma_8(\frac{5}{2})$
Γ_6	$-42.6^a - 10.4^b$			
Γ_7		$+25.6^a - 29.6^b$		
$\Gamma_8(\frac{3}{2})$			$-17.06^a - 23.8^b$	$+2.53^b$
$\Gamma_8(\frac{5}{2})$				$+25.6^a - 25.8^b$
ZnS				
Γ_6	$-44.25^a - 10^b$			
Γ_7		$+26.55^a - 29.2^b$		
$\Gamma_8(\frac{3}{2})$			$-17.7^a - 23.5^b$	$+2.62^b$
$\Gamma_8(\frac{5}{2})$				$+26.55^a - 25.3^b$

effect, the above formulas give the following RDS's:

$$\mathcal{G}[^6A_1 \rightarrow \Gamma_6(^4T_1)] = 45, \quad \mathcal{G}[^6A_1 \rightarrow \Gamma_7(^4T_1)] = 20,$$

$$\mathcal{G}[^6A_1 \rightarrow \Gamma_8(\tfrac{3}{2})(^4T_1)] = 63, \quad \mathcal{G}[^6A_1 \rightarrow \Gamma_8(\tfrac{5}{2})(^4T_1)] = 22$$

for the transitions from the $^6A_1$ level to the fine-structure lines of a $^4T_1$ state in T_d symmetry ($P = 0$).

IV. COMPARISON WITH EXPERIMENTS

For Mn^{++} in ZnSe, the electronic structure of the lowest $^4T_1$ level was calculated from the following values of the Racah parameters and of the cubic field parameter[11]: $B = 740\ cm^{-1}$, $C = 2740\ cm^{-1}$, and $Dq = -405\ cm^{-1}$. The nonreduced first-order and second-order spin-orbit contributions are given in Table II, and the dipole strengths are given in Sec. III C. Obviously this structure is in disagreement with experiments.

As suggested by the experimental results, we will now consider a strong coupling to an E vibrational mode. In that case, f_a, f_b, and $e^{-x/2}$ are approximately zero and the theoretical spectrum is reduced to two "zero-phonon lines" corresponding to transitions from the $^6A_1$ state to the almost degenerate vibronic states:

$$|\Gamma_7, 00\rangle \text{ and } (3/\sqrt{10})|\Gamma_8(\tfrac{3}{2}), 00\rangle - (1/\sqrt{10})|\Gamma_8(\tfrac{5}{2}), 00\rangle$$

for the states at lower energy, and

$$|\Gamma_6, 00\rangle \text{ and } (1/\sqrt{10})|\Gamma_8(\tfrac{3}{2}), 00\rangle + (3/\sqrt{10})|\Gamma_8(\tfrac{5}{2}), 00\rangle$$

for the states at higher energy. The splitting of the two "zero-phonon lines" is due to the nonreduced matrix elements of the second-order spin-orbit interactions. Taking into account all the relevant multiplets of the d^5 configuration, this splitting is calculated to be $7.4\ cm^{-1}$.[19] (This value was obtained by nulling f_a, f_b, and $e^{-x/2}$.) *The best argument in favor of this model is that it predicts correctly the uniaxial stress effects.*

The pressure effects reported in Fig. 2 were correctly fitted by taking $\mathcal{C}_{ZnSe} = 4800\ cm^{-1}$ per unit strain (see Table III), the shift common to all lines being $17\,800\ cm^{-1}$ per unit strain. (The used elastic constants were those of the pure crystal determined by Berlincourt *et al.*[20] at 25 °C: $s_{11} = 2.26 \times 10^{-12}$ cm^2/dyn, and $s_{12} = -0.85 \times 10^{-12}\ cm^2/dyn$.)

The calculated RDS's for a zero applied pressure and the polarization effects under pressure reported in Fig. 2 are in good agreement with experiments. In fact, it is necessary to be aware of the different linewidths of the two lines at higher energy and of the two lines at lower energy before comparing the calculated RDS's to experiments. The slight broadening of the lines at lower energy is obviously due to the greater sensitivity of these lines to uniaxial strain (see Fig. 2).

In the case of Mn^{++} in ZnS, the chosen values of B, C, and Dq are $B = 730\ cm^{-1}$, $C = 2880\ cm^{-1}$, and $Dq = -420\ cm^{-1}$.[10] The first- and second-order spin-orbit contributions are given in Table II. In the limit of a strong Jahn-Teller coupling to an E vibrational mode, the calculated spectrum consists of two lines separated by $7.7\ cm^{-1}$.[19] Of course the wave functions of the fundamental vibronic states are identical to those of Mn^{++} in ZnSe.

The shifts and splittings of the lines in terms of the applied pressure (Fig. 4) are correctly fitted with $\mathcal{C}_{ZnS} = 5400\ cm^{-1}$ per unit strain, the shift common to all levels being $23\,600\ cm^{-1}$ per unit strain[20]

($s_{11} = 1.786 \times 10^{-12}$ cm^2/dyn, $s_{12} = 0.685 \times 10^{-12}$ cm^2/dyn at 77 K).

As pointed out in Sec. II B, the behavior under stress of the two lines centered at 18 015 cm^{-1} due to the Mn^{++} centers in stacking faults is identical to that of cubic centers (same shift and same $\mathcal{C}$ parameter). The Mn^{++} centers giving the four zero-phonon lines centered at 17 990 cm^{-1} are obviously not as strongly coupled to the lattice as the cubic centers. Actually, the nature of these Mn^{++} centers is not well known enough to permit an analysis of the Jahn-Teller effect.

The experimental data obtained on cubic centers support the hypothesis of a strong Jahn-Teller coupling with an E mode made by Fournier *et al.* in order to explain the Zeeman splitting anisotropy of the $^4T_1$ relaxed excited state.[9] Although the present formalism carried in cubic symmetry is particularly able to express the wave functions when going from intermediate to strong coupling, the stress data could also be easily interpreted using the tetragonal anisotropic centers in cubic crystals formalism[21] in order to represent, as in Ref. 9, the three tetragonal distortions in the static limit.

V. COMPARISON OF THE JAHN-TELLER EFFECT IN THE LOWEST $^4T_1$ AND $^4T_2$ STATES OF Mn^{++} IN ZnS AND ZnSe

Although the adopted structure for the fluorescent $^4T_1$ levels of ZnSe : Mn and cubic ZnS : Mn permits a very good interpretation of all experimental results, several difficulties arise when comparing the Jahn-Teller effect in the lowest $^4T_1$ and $^4T_2$ levels. [For the lowest $^4T_2$ levels of Mn^{++} in ZnSe and ZnS, the values of the Huang-Rhys factors S and of the strengths of the couplings to an E vibrational mode are[6]: $S(^4T_2) = 1.2$ for ZnSe; $S(^4T_2) = 0.6$ for ZnS; $V_E = A_{ZnSe} = -3650$ cm^{-1} for ZnSe : Mn; and $V_E = A_{ZnS} = -3100$ cm^{-1} for ZnS : Mn.]

In fact, in the case of a very strong Jahn-Teller coupling, uniaxial stress experiments alone do not permit a precise determination of the strength of the coupling. Stress and magnetic circular dichroism experiments performed on the zero-phonon lines and on the broad bands could have given the Huang-Rhys factor S and the frequency of the effective phonon. Unfortunately, given the small absorption of the $^6A_1 \rightarrow {}^4T_1$ bands, the dichroism experiments performed on the crystals at our disposal failed to give an experimental estimate for S.

However, it is possible to evaluate S for the fluorescent levels by assuming that the nearest-neighbor cluster model is valid and that the frequencies of the effective phonons are equal in the $^4T_1$ and $^4T_2$ states (so that $S \propto V_E^2$). From these hypotheses and the values of S and V_E for the $^4T_2$ states, we get $S(^4T_1) = 2$ for ZnSe : Mn, and $S(^4T_1) = 1.8$ for ZnS : Mn. These values represent a lower limit of S to account for the strong quenching of the spin-orbit splittings in the studied fluorescent levels; in fact, they are in agreement with a crude estimate of the lower limit of S obtained from the ratio of the unquenched spin-orbit splitting to the linewidth [this estimate gives $S(^4T_1) \sim 1.8$ for ZnSe : Mn, and $S(^4T_1) \sim 1.9$ for ZnS : Mn]. Higher values for the Huang-Rhys factors in the $^4T_1$ states could be obtained by assuming that the frequencies of the effective phonons are smaller in the $^4T_1$ states than in the $^4T_2$ states; however, no experimental proof of this hypothesis is actually available.

Finally, the coupling parameters for the $^4T_1$ and $^4T_2$ states have been calculated in a crystal-field model (see Appendix). We obtained

$$\mathcal{C}_{ZnS} = -604 \text{ cm}^{-1} \text{ (exp: } -5400 \text{ cm}^{-1}),$$

$$\mathcal{C}_{ZnSe} = -484 \text{ cm}^{-1} \text{ (exp: } -4800 \text{ cm}^{-1})$$

for the $^4T_1$ levels, and

$$A_{ZnS} = -1757 \text{ cm}^{-1} \text{ (exp: } -3100 \text{ cm}^{-1})^6,$$

$$A_{ZnSe} = -1475 \text{ cm}^{-1} \text{ (exp: } -3650 \text{ cm}^{-1})^6$$

for the $^4T_2$ levels. These values show that the crystal-field model gives no more than an order-of-magnitude agreement between the calculated and the measured coupling parameters so that this model is of little help in predicting the strength of the coupling to an E vibrational mode. Furthermore, this model predicts that the coupling of the $^4T_1$ state to the T_2 vibrational modes should be stronger than the coupling to the E mode in the case of ZnSe : Mn and ZnS : Mn, although the exper-

TABLE III. Matrix elements of the pressure-induced crystal field for $\vec{P} \| [100]$. The α' ($\mathcal{C}\tau J$) and β' ($\mathcal{C}\tau J$) are, respectively, the diagonal and off-diagonal (in Td*) matrix elements of the spin-orbit interaction. The parameter $\mathcal{C}$ is defined in Sec. III.

	$\Gamma_6 \pm \frac{1}{2}$	$\Gamma_8(\frac{3}{2}) \pm \frac{1}{2}$	$\Gamma_8(\frac{5}{2}) \pm \frac{1}{2}$
$\Gamma_6 \pm \frac{1}{2}$	$\alpha'(\Gamma_6)$	$\pm (1/2\sqrt{5})\,\mathcal{C}$	$\pm (3/2\sqrt{5})\,\mathcal{C}$
$\Gamma_8(\frac{3}{2}) \pm \frac{1}{2}$		$\alpha'[\Gamma_8(\frac{3}{2})] + \frac{2}{5}\mathcal{C}$	$\beta' - \frac{3}{10}\mathcal{C}$
$\Gamma_8(\frac{5}{2}) \pm \frac{1}{2}$			$\alpha'[\Gamma_8(\frac{5}{2})] - \frac{2}{5}\mathcal{C}$
	$\Gamma_7 \pm \frac{1}{2}$	$\Gamma_8(\frac{3}{2}) \mp \frac{3}{2}$	$\Gamma_8(\frac{5}{2}) \mp \frac{3}{2}$
$\Gamma_7 \pm \frac{1}{2}$	$\alpha'(\Gamma_7)$	$\mp (3/2\sqrt{5})\,\mathcal{C}$	$\pm (1/2\sqrt{5})\,\mathcal{C}$
$\Gamma_8(\frac{3}{2}) \mp \frac{3}{2}$		$\alpha'[\Gamma_8(\frac{3}{2})] - \frac{2}{5}\mathcal{C}$	$\beta' + \frac{3}{10}\mathcal{C}$
$\Gamma_8(\frac{5}{2}) \mp \frac{3}{2}$			$\alpha'[\Gamma_8(\frac{5}{2})] + \frac{2}{5}\mathcal{C}$

imental results show that the coupling to the T_2 modes is negligible.

VI. CONCLUSION

As a preliminary result, the zero-phonon lines of the fluorescent level of Mn^{++} in ZnSe were observed unambiguously for the first time. Then from a very detailed experimental study under stress of the fluorescent $^4T_1$ states of Mn^{++} in ZnSe and ZnS (cubic centers) it was shown directly that these states are strongly coupled to an E vibrational mode. A structure for the observed lines was established permitting us to interpret all experimental results (splitting under stresses, relative dipole strengths, and polarization effects under stresses).

A comparison with the results previously obtained for the lowest $^4T_2$ states of Mn^{++} in ZnSe and ZnS,[6] has shown that the structure of the $^4T_1$ and $^4T_2$ states are very different, although the spectra of the zero-phonon lines (for $P=0$) are identical in the case of ZnSe : Mn and differ only by the energy separation of the zero-phonon lines in the case of ZnS: Mn. This comparison led us to determine a lower limit for the Huang-Rhys parameters in the fluorescent levels of Mn^{++} in ZnSe and ZnS, and to emphasize the problems encountered when trying to compare the Jahn-Teller couplings in the $^4T_1$ and $^4T_2$ states.

ACKNOWLEDGMENTS

Thanks are due to Dr. M. D. Sturge for a very critical reading of the manuscript. We are also indebted to Dr. R. Romestain for giving us the ZnSe : Mn crystals used in this work and to N. Machorine, A. Vandenborghe, and P. Villermet for cutting and polishing the samples used in our experiments.

APPENDIX

The coupling parameters for the $^4T_1$ and $^4T_2$ levels are defined by

$$\mathcal{C} = -\langle {}^4T_1 \| \Delta V(E_u) \| {}^4T_1 \rangle / \epsilon(E_u)$$

and

$$A = -\langle {}^4T_2 \| \Delta V(E_u) \| {}^4T_2 \rangle / \epsilon(E_u) ,$$

where

$$\Delta V(E_u) = \Delta B_2 D_0^{(2)} + \Delta B_4 [D_0^{(4)} - (\sqrt{7}/\sqrt{10})(D_4^{(4)} + D_{-4}^{(4)}] .$$

The $D^{(k)}$'s are electronic operators defined in terms of radial integrals and spherical harmonics by

$$D^{(k)} = [4\pi/(2k+1)]^{1/2} \langle 3d|r^k|3d\rangle Y^{(k)} .$$

The ΔB_k's are stress-induced crystal-field parameters linear in $\epsilon(E_u)$.

By writing the $^4T_1$ and $^4T_2$ states in terms of spectroscopic terms, we obtain

$$\mathcal{C} = -(4|e|/3\sqrt{5})\gamma(2\alpha+\beta) \times [\Delta B_4/\epsilon(E_u)] \langle 3d|r^4|3d\rangle$$

and

$$A = +(4|e|/21\sqrt{7})\beta'(2\alpha' + \sqrt{3}\,\gamma') \times \{[6\Delta B_2/\epsilon(E_u)] \langle 3d|r^2|3d\rangle - [\Delta B_4/\epsilon(E_u)] \langle 3d|r^4|3d\rangle\} ,$$

where the mixing parameters α, β, γ and α', β', γ' are defined by

$$|{}^4T_1\rangle = \alpha|{}^4P\rangle + \beta|{}^4F\rangle + \gamma|{}^4G\rangle ,$$

$$|{}^4T_2\rangle = \alpha'|{}^4D\rangle + \beta'|{}^4F\rangle + \gamma'|{}^4G\rangle .$$

By evaluating ΔB_2 and ΔB_4 in a point-charge model restricted to the nearest neighbors we get

$$\Delta B_2 = -|e|(8/3R^3)\epsilon(E_u)$$

and

$$\Delta B_4 = +|e|(40/27R^5)\epsilon(E_u),$$

where R is the nearest-neighbor distance.

The values for $\mathcal{C}$ and A given in Sec. V were obtained from the following data: $\langle 3d|r^4|3d\rangle = 5.513a_0^4$ (a_0 is the first Bohr radius), $\langle 3d|r^2|3d\rangle = 1.548a_0^2$ for[22] Mn^{++}; $R = 4.43a_0$,[23] $\alpha' = 0.112\,39$, $\beta' = 0.200\,99$, $\gamma' = 0.973\,13$ for ZnS : Mn, and $R = 4.638a_0$[23]; $\alpha' = 0.104\,62$, $\beta' = 0.195\,15$, and $\gamma' = 0.975\,18$ for ZnSe : Mn.

---

*Equipe de Recherche associée au CNRS.

†Equipe de Recherche No. 5 du CNRS.

[1]See, for example M. D. Sturge, in *Solid State Physics*, edited by F. Seitz and G. Turnbull (Academic, New York, 1967), Vol. 20; A. Abragam and B. Bleaney, *Electron Paramagnetic Resonance of Transition Metal Ions* (Clarendon, Oxford, 1969); R. Englman, *The Jahn-Teller Effect in Molecules and Crystals* (Wiley, New York, 1972); F. S. Ham, in *Electron Paramagnetic Resonance*, edited by S. Geschwind (Plenum, 1972).

[2]R. Romestain, thesis (University of Paris, 1972) (unpublished).

[3]A. Landi, C. Blanchard, and R. Parrot, Phys. Lett. A 36, 267 (1971).

[4]M. Y. Chen, D. S. McClure, and E. I. Solomon, Phys. Rev. B 6, 1690 (1972).

[5]E. I. Solomon and D. S. McClure, Phys. Rev. B 6, 1697

(1972); 9, 4690 (1974).
[6]R. Parrot, C. Naud, and F. Gendron, Phys. Rev. B 13, 3748 (1976).
[7]F. S. Ham and G. A. Slack, Phys. Rev. B 4, 777 (1971).
[8]P. Koidl, Phys. Status Solidi 74, 477 (1976).
[9]D. Fournier, A. C. Boccara, and J. C. Rivoal, J. Phys. C 10, 113 (1977).
[10]R. Parrot and C. Blanchard, Phys. Rev. B 6, 3992 (1972).
[11]D. Langer and H. J. Richter, Phys. Rev. 146, 554 (1966).
[12]M. Zigone, R. Beserman, and B. Lambert, J. Lumin. 9, 45 (1974).
[13]F. S. Ham, Phys. Rev. 138, A1727 (1965).
[14]J. S. Griffith, *The Irreducible Tensor Method for Molecular Symmetry Groups* (Prentice-Hall, Englewood Cliffs, N. J., 1962).
[15]In Ref. 6, p. 3753, replace the sentence: "The complete calculation must be performed by taking into account all 35 relevant multiplets $^4T_1(3)$, $^4T_2(3)$, $^2E(7)$, $^2T_1(8)$, $^2T_2(10)$, $^2A_2(3)$, $^4A_2(1)$ of the d^5 configuration ..." by "The complete calculation must be performed by taking into account all 37 relevant multiplets $^4E(2)$, $^4T_1(3)$, $^4T_2(3)$, $^2E(7)$, $^2T_1(8)$, $^2T_2(10)$, $^2A_2(3)$, $^4A_2(1)$ of the d^5 configuration ... ."
[16]A. I. Schawlow, A. H. Piksis, and S. Sugano, Phys. Rev. 122, 1469 (1961).
[17]M. Vala, J. C. Rivoal, and J. Badoz, Mol. Phys. 30, 1325 (1975).
[18]J. Schneider, S. R. Sircar and A. Rauber, Z. Naturforsch A 18, 980 (1963).
[19]The contribution of the spin-spin interactions is not included in this value. This contribution is less than 1 cm^{-1} in the case of Mn^{++} in ZnSe and ZnS (from Ref. 8).
[20]Don Berlincourt, H. Jaffe, and L. R. Shiozawa, Phys. Rev. 129, 1009 (1963).
[21]A. E. Hughes and W. A. Runciman, Proc. Phys. Soc. Lond. 90, 827 (1967).
[22]M.Blume and R. Orbach, Phys. Rev. 127, 1587 (1962).
[23]M. Aven and J. S. Prener, *Physics and Chemistry of II-VI Compounds* (North-Holland, Amsterdam, 1967).